Liu *et al. Biomarker Research* (2026) 14:52
https://doi.org/10.1186/s40364-026-00931-1

Biomarker Research

CORRESPONDENCE Open Access

Single-cell transcriptomic mapping of immune heterogeneity across angioimmunoblastic T-cell lymphoma subtypes

Huimin Liu[1,2†], Yang Tong[1,2†], Meijuan Wu[3†], Zhuoxin Zhang[1,2], Yao Yao[1,2], Zhanqi Li[1,2], Yin Shi[1,2], Zhen Yu[1,2], Gang An[1,2], Lugui Qiu[1,2], Yang Yang[4,5*], Haiyan Yang[3*], Dehui Zou[1,2*] and Jiapei Yuan[1,2*]

Abstract

Relapse and treatment resistance remain critical obstacles in the clinical management of angioimmunoblastic T-cell lymphoma (AITL), limiting the success of current therapeutic strategies. Therefore, a comprehensive characterization of the tumor microenvironment (TME) in AITL is essential to enhance treatment efficacy. This study analyzed samples from 68 patients with AITL, stratified into three molecular subtypes based on immunoglobulin (IG) gene rearrangement and flow cytometry results. Utilizing single-cell RNA sequencing, the TME was profiled across subtypes A, B, and C, sampling multiple disease sites including the bone marrow, lymph nodes, and peripheral blood. Our findings revealed subtype-specific variations in cellular composition and transcriptional programs within the TME. Unlike other subtypes, subtype C was associated with a pronounced immunosuppressive environment at diagnosis and relapse. Additionally, it exhibited an enhanced response to Epstein–Barr virus infection, consistent with upregulated *CD70* expression at relapse. Through the analysis of cellular communication networks, CD70, programmed cell death 1 (PDCD1), and inducible T cell costimulator (ICOS) were identified as promising immunotherapeutic targets in AITL. Finally, we delineated distinct cellular proportions and gene expression signatures characteristic of each subtype, providing a foundation for the development of tailored therapeutic interventions for patients with AITL.

†Huimin Liu, Yang Tong and Meijuan Wu contributed equally to this work.

*Correspondence:
Yang Yang
yy@tmu.edu.cn
Haiyan Yang
yanghy@zjcc.org.cn
Dehui Zou
zoudehui@ihcams.ac.cn
Jiapei Yuan
yuanjiapei@ihcams.ac.cn

Full list of author information is available at the end of the article

Keywords Angioimmunoblastic T-cell lymphoma, Spatial heterogeneity, Longitudinal profiling, Tumor microenvironment

To the Editor

Angioimmunoblastic T-cell lymphoma (AITL) is an aggressive, heterogeneous type of peripheral T-cell lymphoma associated with poor outcomes; currently, there is no standard therapy for this disease [1–3]. AITL is characterized by the presence of few neoplastic T follicular helper (Tfh) cells within a complex inflammatory tumor microenvironment that includes Epstein–Barr virus-positive (EBV+) B cells, plasma cells, and follicular dendritic cells [4, 5]. Approximately 25–30% of cases show clonal IG rearrangement [6, 7]. Although prior studies reported B-cell expansion, they lacked subtype-specific and longitudinal resolution [4, 8, 9]. We prospectively stratified 68 AITL cases into three molecular subtypes based on immunoglobulin (IG) gene rearrangement of involved lymph nodes and diagnostic bone marrow flow cytometry: A ($n = 47$, monoclonal T cells only); B ($n = 19$, simultaneous clonal IG rearrangement); and C ($n = 2$, concurrent monoclonal B and plasma cells) (Fig. 1A). Subtype B exhibited a non-significant trend toward improved survival versus subtype A (Fig. S1 ; Table S1). Two subtype C cases had advanced EBV+ AITL featuring pathologically confirmed clonal IG rearrangements and aberrant T/B/plasma cell phenotypes (Figs. S2, S3).

Compartmentalization of immune and malignant cells in AITL subtypes

Longitudinal single-cell RNA sequencing was performed with paired T-cell receptor/B-cell receptor (TCR/BCR) V(D)J data on bone marrow, lymph node, and peripheral blood samples obtained from 16 patients with AITL at diagnosis, remission, and relapse (Fig. S4 ; Table S2). Integration revealed 16 cell clusters and marked subtype-, stage- and lesion-specific remodeling (Fig. 1B, C). Within compartments, we defined three malignant subtypes, 11 T-cell subclusters, and 10 monocyte subclusters (Fig. S5). Subtypes A/B had higher abundance of effector CD8+ and γδ T cells than subtype C (Fig. 1D). Subtype C featured abundant malignant B/plasma cells and depleted Tfh cells (Fig. 1E–H). Within the T-cell subclusters (Fig. 1I–J), RAS guanyl releasing protein 1 (*RASGRP1*), Janus kinase 3 (*JAK3*), and PR/SET domain 1 (*PRDM1*) were enriched at diagnosis in subtype C, consistent with transcriptional programs associated with T-cell responses to EBV infection (Fig. 1K) [10]. In patient C01, malignant B/plasma cells dominated marrow and blood, while malignant Tfh cells were concentrated in lymph node samples; effector CD8+ and regulatory T (Treg) cells were enriched in lymph node samples, indicating earlier Tfh/immune dominance (Fig. 1L; S6). Immunostaining and flow cytometry confirmed abnormal T/B/plasma subsets across lesions (Fig. 1M, N; S2, S3).

Subtype- and stage-specific tumor microenvironment dynamics in AITL treatment

Approximately 70% of AITL cases exhibit bone marrow involvement; therefore, we recently compared immune compositions in bone marrow samples [3]. In C01, malignant Tfh cells expanded markedly at relapse, while malignant B and plasma cells declined after chemotherapy and did not recur (Fig. 2A; S7). In contrast, A01 and A02 displayed notable shifts in B/plasma compartments despite no B-cell-targeted therapy. Malignant program 1, enriched for B-cell proliferation/activation genes (*CD22*, *CD86*, *FGR*), was highest in C01 at diagnosis and declined during remission (Fig. 2B–D). Malignant T-cell programs linked to TCR signaling (linker for activation of T cells [*LAT*], lymphocyte-specific protein tyrosine kinase [*LCK*]) decreased in remission and rebounded at relapse in A01/A02 (consistent with immune reactivation); however, they remained suppressed at relapse in C01 (Fig. 2E–G). Monocyte counts diverged at relapse; C01 showed a decrease, whereas A01/A02 showed an increase, with inflammatory and EBV related signatures (Fig. 2H–J ; S8, S9). T-cell remodeling also differed; in C01, remission featured increased effector CD8+ cells that declined at relapse, whereas Treg cells rose at relapse, suggesting immunosuppression; A01/A02 retained stable

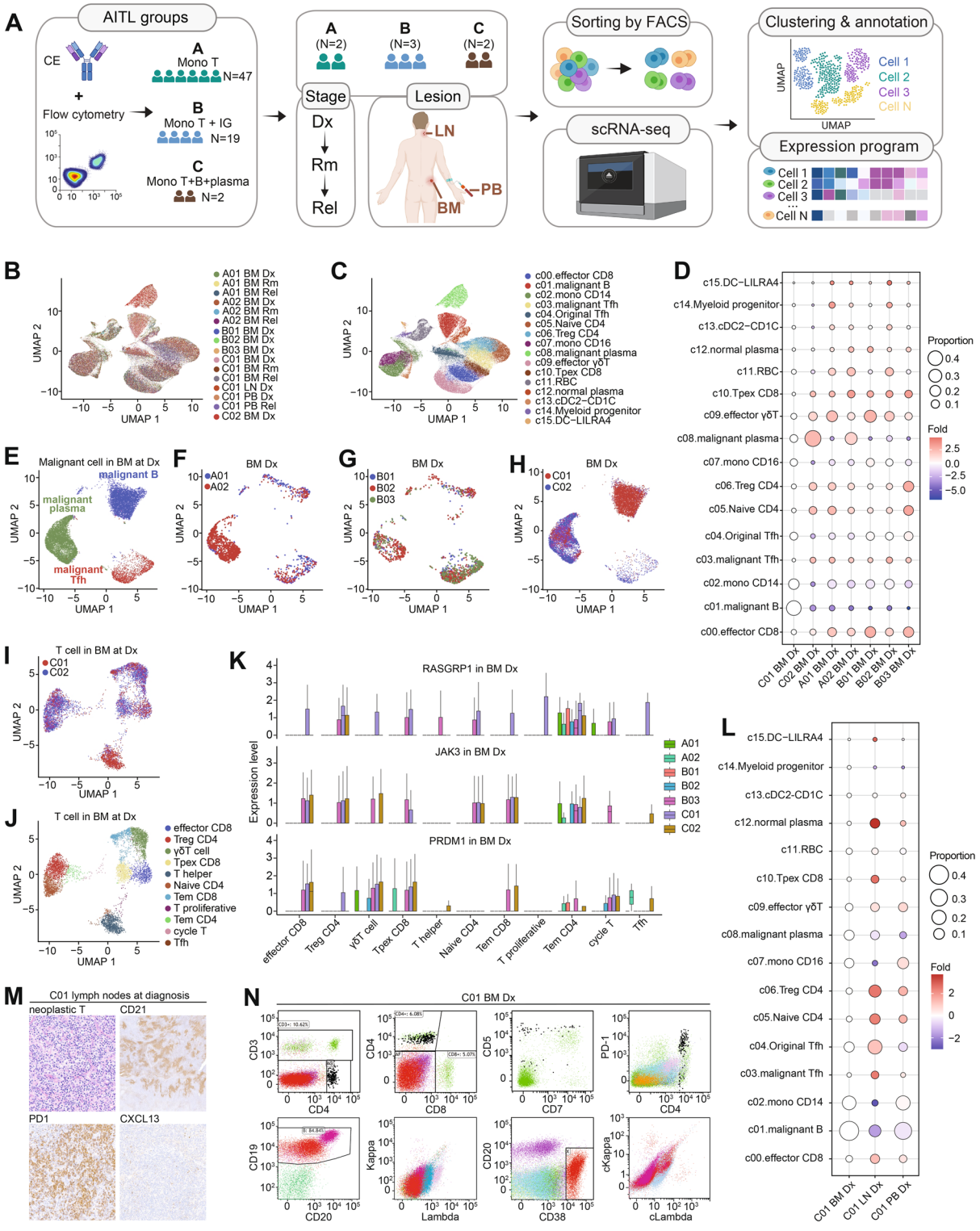

Fig. 1 (See legend on next page.)

(See figure on previous page.)

Fig. 1 Immune microenvironment heterogeneity in AITL across molecular subtypes. (**A**) Study design schematic, including sample sources (LN, lymph node; BM, bone marrow; PB, peripheral blood) and clinical timepoints (Dx, diagnosis; Rm, remission; Rel, relapse). (**B**) UMAP analysis integrating all 16 single-cell datasets. (**C**) UMAP visualization of 16 distinct cell populations identified in the AITL microenvironment. (**D**) Proportional shifts in immune cell composition across AITL subtypes. Circle size reflects cell abundance; color indicates fold-change relative to the bone marrow of patient C01 at diagnosis. (**E**) UMAP projection of malignant cell clusters in the cohort. (**F**-**H**) Subtype-specific UMAP plots of malignant cells at diagnosis, stratified by patient ID (subtypes A, B, and C). (**I**) UMAP of T cells in subtype C at diagnosis, annotated by patient ID. (**J**) Corresponding T-cell subclusters in subtype C, color-coded by cell identity. (**K**) Boxplots showing the expression dynamics of *RASGRP1*, *JAK3*, and *PRDM1* across T-cell subpopulations in AITL patients. (**L**) Proportional distribution of major cell populations in lymph node (LN), bone marrow (BM), and peripheral blood (PB) samples from C01 at diagnosis. (**M**) Pathological results of left cervical lymph nodes in C01: (i) hematoxylin-eosin staining, ×400: neoplastic T cells with abundant, clear cytoplasm and notable high-endothelial venule hyperplasia. (ii) Immunohistochemical staining (IHC), ×40: irregular expansion of the follicular dendritic cell (FDC) network. (iii) IHC, PD-1, ×400: tumor T cells show PD-1 positivity. (iv) IHC, CXCL13, ×100: CXCL13 expression in partial positive neoplastic T cells. (**N**) In bone marrow from C01 at diagnosis, three abnormal populations were detected: (1) CD3–CD4+CD8–PD1+ T cells with partial CD7 expression (black); (2) CD19+CD20+CD38– B cells lacking surface kappa and lambda light chains (dark purple); and (3) CD38+CD19+CD20– plasma cells negative for cytoplasmic kappa and lambda (red)

T-cell proportions (Fig. 2K–L ; S10). Distinct transcriptional programs were mapped to subsets: a cytotoxic program (granzyme B [*GZMB*], granulysin [*GNLY*]) localized to γδ and effector memory- CD8+ T cells (Fig. 2M–O); a CD4-enriched TCR signaling/differentiation program (Fig. S11); and a viral-response program in exhausted CD8+ cells suggested tumor-suppressive activity (Fig. S12).

Post-treatment cellular interactions across AITL subtypes

Longitudinal analysis revealed increased interactions between malignant Tfh cells, effector γδ T cells, and Treg cells in C01, implicating resistance-associated signaling (Fig. S13). Ligand–receptor profiling identified conserved versus stage-restricted mediators; fms-related receptor tyrosine kinase 3 (FLT3) interactions occurred at diagnosis and remission but not at relapse (Fig. 2P, Q). CD70, linked to EBV-driven T cell responses and absent pre-relapse, was enriched in Treg cells and progenitor exhausted-T CD8+ cells at relapse and correlated with intensified Tfh–T-cell crosstalk (Fig. 2R, S); programmed cell death-ligand 1 (PD-L1) similarly supported an immunosuppressive microenvironment (Fig. 2T). Patient A01 showed variable Tfh–monocyte crosstalk and shifts in mediators (FLT3, inducible T cell costimulator [ICOS]/CD28) (Fig. S14). Clonality analyses paralleled these changes; C01 maintained hyperexpanded BCR/TCR clones across stages, whereas A01/A02 showed contraction at remission (Fig. S15).

This exploratory longitudinal single-cell study revealed subtype-specific molecular and immune heterogeneity in AITL; future work requires larger prospective cohorts with well-defined tissue sources and robust statistical power to validate these findings.

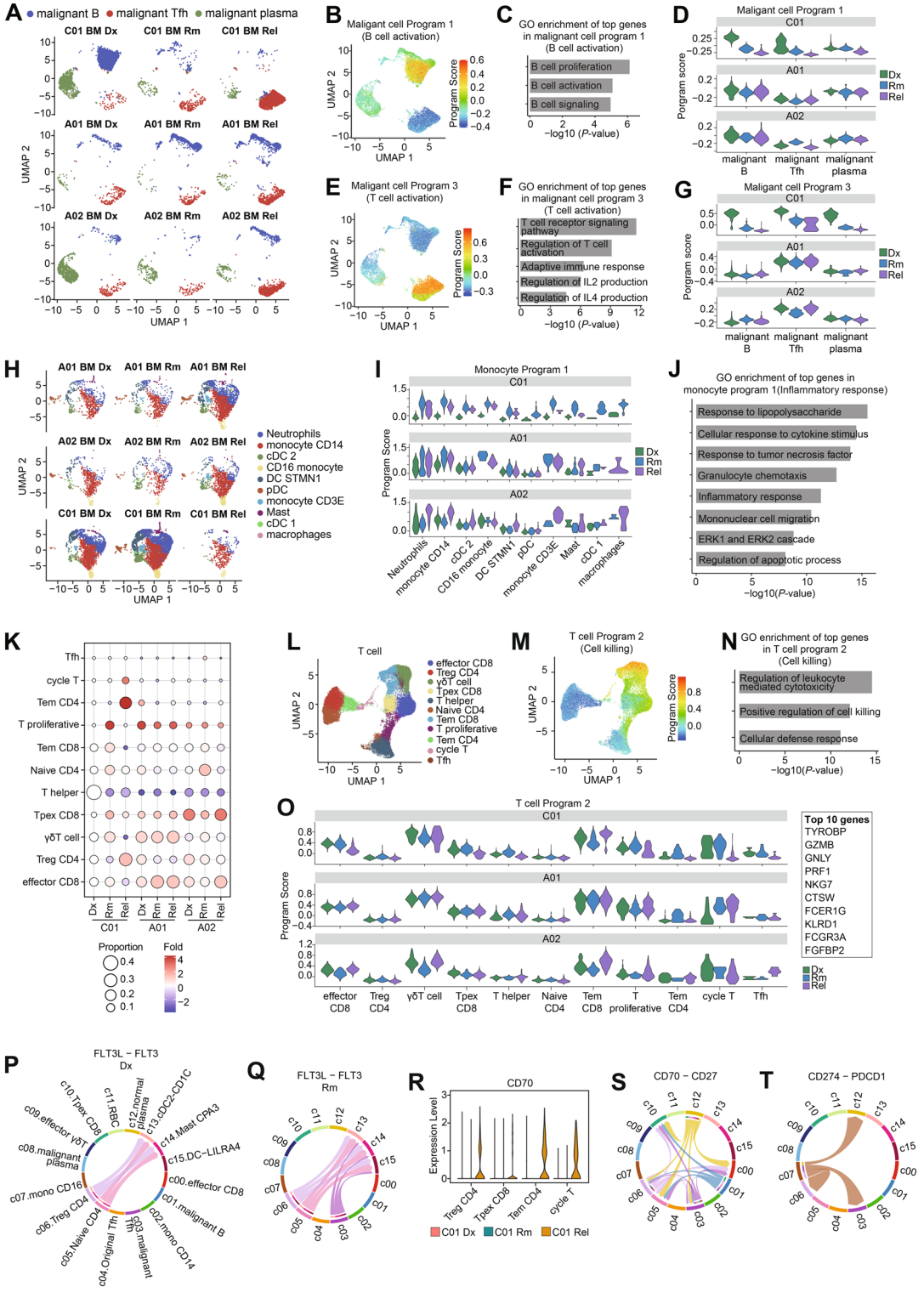

Fig. 2 (See legend on next page.)

(See figure on previous page.)

Fig. 2 Longitudinal characterization of cell proportions and transcriptional landscapes across AITL subtypes. (**A**) UMAP visualization of malignant cells derived from two subtype A patients (A01 and A02) and one subtype C patient (C01), encompassing bone marrow samples collected at diagnosis, remission, and relapse. (**B**) UMAP embedding based on the expression profiles of the top 100 genes in malignant cell program 1. (**C**) GO enrichment analysis of the top 100 genes within program 1. (**D**) Quantification of program 1 activity scores across malignant cells from AITL patients. (**E**) UMAP visualization reflecting the expression of the top 100 genes in program 3. (**F**) GO enrichment analysis of the program 3 gene set. (**G**) Program 3 activity scores mapped onto malignant cells from all patients. (**H**) Quantitative assessment of the relative abundance of monocyte subsets across disease stages stratified by AITL subtype. (**I**) Longitudinal analysis of P1 program scores at diagnosis, remission, and relapse. (**J**) GO enrichment analysis of the top 100 genes in P1. (**K**) Quantitative analysis showing the relative proportions of distinct T cell subsets across different disease stages within AITL subtypes. (**L**) UMAP representation colored according to identified T cell subclusters. (**M**) UMAP clustering based on the expression profiles of the top 100 genes defining T cell program 2. (**N**) GO enrichment analysis of the top 100 genes in expression program 2 (P2). (**O**) Expression program scores of the top 100 P2 genes (left) and the lists of the top 10 P2 genes (right) at diagnosis, remission, and relapse. (**P**-**Q**) characterization of FLT3L-FLT3 axis-mediated interactions at diagnosis and remission in patient C01. (**R**) Expression patterns of *CD70* across T cell subpopulations at diagnosis, remission, and relapse. (**S**) CD70–CD27 interactions mediating cell-cell communication at relapse in patient C01. (**T**) Dynamics of CD274–PDCD1 mediated interactions at relapse in patient C01

Abbreviations

AITL	Angioimmunoblastic T-cell lymphoma
TME	Tumor microenvironment
scRNA-seq	Single-cell RNA sequencing
EBV	Epstein-Barr virus
IG	Immunoglobulin
TFH	Follicular helper T cells
LN	Lymph node
BM	Bone marrow
PB	Peripheral blood
IHC	Immunohistochemical staining
FDC	Follicular dendritic cell
PFS	Progression-free survival
OS	Overall survival

Supplementary Information

The online version contains supplementary material available at https://doi.org/10.1186/s40364-026-00931-1.

Supplementary material 1

Supplementary material 2

Supplementary material 3

Supplementary material 4

Acknowledgements

We gratefully acknowledge the technical support of the High-performance Computing Platform of Tianjin Medical University.

Author contributions

Conception and design: H.L., D.Z., and J.Y.; Development of methodology: H.L., Y.T., Y.Y., D.Z. and J.Y.; Acquisition of data: H.L., Y.T., M.W., Z.Z., Y.Y., Z.L., Y.S., Z.Y., G.A.; Analysis and interpretation of data: H.L., Y.T., L.Q., Y.Y., H.Y., and J.Y.; Writing, review, and/or revision of the manuscript: H.L. and J.Y. with input from all authors; Study supervision: D.Z. and J.Y.

Funding

The current work was supported by the following grants: the Chinese Academy of Medical Sciences (CAMS) Innovation Fund for Medical Sciences (2024-I2M-C&T-B-083 to H.L., 2023-I2M-3-004, 2023-I2M-2-007 and 2022-I2M-2-003 to J.Y.), the National Natural Science Foundation of China (82400237 to H.L., 32200514 to J.Y. and 32470721 to Y.Y.), Tianjin Youth Science and Technology Talent Project (QN20230324 to Y.Y.) and the Natural Science Foundation of Tianjin Municipality (24JCYBJC00960 to Y.Y.).

Data availability

The raw sequence data generated by this study have been deposited in the Genome Sequence Archive (GSA-Human: HRA012628), which are publicly accessible at https://ngdc.cncb.ac.cn/gsa-human.

Declarations

Ethics approval and consent to participate

Ethical approval was granted by the Ethics and Human Research Committees of the Institute of Hematology & Blood Disease Hospital (CAMS & PUMC) and Zhejiang Cancer Hospital (approvals IIT2021030-EC-1 and IRB-2018-105). All procedures involving human participants were conducted in accordance with the ethical standards of the institutional research committees and with the Declaration of Helsinki.

Consent for publication

The authors confirm that they have obtained written consent from each patient to publish the manuscript.

Competing interests

The authors declare no competing interests.

Author details

[1]State Key Laboratory of Experimental Hematology, National Clinical Research Center for Blood Diseases, Haihe Laboratory of Cell Ecosystem, Institute of Hematology & Blood Diseases Hospital, Chinese Academy of Medical Sciences & Peking Union Medical College, Tianjin 300020, China
[2]Tianjin Institute of Health Science, Tianjin 301600, China
[3]Zhejiang Cancer Hospital, Hangzhou Institute of Medicine (HIM), Chinese Academy of Sciences, Hangzhou, Zhejiang 310022, China
[4]The Province and Ministry Co-Sponsored Collaborative Innovation Center for Medical Epigenetics, State Key Laboratory of Experimental Hematology, Tianjin Key Laboratory of Inflammatory Biology, Department of Bioinformatics, School of Basic Medical Sciences, Tianjin Medical University, Tianjin 300070, China
[5]Department of Pharmacology, School of Basic Medical Sciences, Tianjin Medical University, Tianjin 300070, China

Received: 16 February 2026 / Accepted: 7 May 2026
Published online: 22 May 2026

References

1. Advani RH, Skrypets T, Civallero M, Spinner MA, Manni M, Kim WS, et al. Outcomes and prognostic factors in angioimmunoblastic T-cell lymphoma: final report from the international T-cell Project. Blood. 2021;138(3):213–20. https://doi.org/10.1182/blood.2020010387.
2. Marchi E, O'Connor OA. The rapidly changing landscape in mature T-cell lymphoma (MTCL) biology and management. CA Cancer J Clinicians. 2020;70(1):47–70. https://doi.org/10.3322/caac.21589.
3. Lunning MA, Vose JM. Angioimmunoblastic T-cell lymphoma: the many-faced lymphoma. Blood. 2017;129(9):1095–102. https://doi.org/10.1182/blood-2016-09-692541.
4. Pritchett JC, Yang ZZ, Kim HJ, Villasboas JC, Tang X, Jalali S, et al. High-dimensional and single-cell transcriptome analysis of the tumor microenvironment in angioimmunoblastic T cell lymphoma (AITL). Leukemia. 2022;36(1):165–76. https://doi.org/10.1038/s41375-021-01321-2.

5. Chiba S, Sakata-Yanagimoto M. Advances in understanding of angioimmunoblastic T-cell lymphoma. Leukemia. 2020;34(10):2592–606. https://doi.org/10.1038/s41375-020-0990-y.
6. Tan BT, Warnke RA, Arber DA. The frequency of B- and T-cell gene rearrangements and epstein-barr virus in T-cell lymphomas: a comparison between angioimmunoblastic T-cell lymphoma and peripheral T-cell lymphoma, unspecified with and without associated B-cell proliferations. J Mol Diagn. 2006;8(4):466–75; quiz 527. https://doi.org/10.2353/jmoldx.2006.060016.
7. Zettl A, Lee SS, Rüdiger T, Starostik P, Marino M, Kirchner T, et al. Epstein-Barr virus–associated B-Cell lymphoproliferative disorders in angioimmunoblastic T-Cell lymphoma and peripheral T-Cell lymphoma, unspecified. Am J Clin Pathol. 2002;117(3):368–79. https://doi.org/10.1309/6UTX-GVC0-12ND-JJEU.
8. Zhu M, Li N, Fan L, Wu R, Cao L, Ren Y, et al. Single-cell transcriptomic and spatial analysis reveal the immunosuppressive microenvironment in relapsed/refractory angioimmunoblastic T-cell lymphoma. Blood Cancer J. 2024;14(1):14. 218. https://doi.org/10.1038/s41408-024-01199-0.
9. Yan WW, Xu JY, Li LN, Lyu R, Shou LH, Sun Q, et al. Angioimmunoblastic T-cell lymphoma with monoclonal B cell and plasma cell hyperplasia. Zhonghua Xue Ye Xue Za Zhi. 2023;44. 783–86.
10. Latour S, Fischer A. Signaling pathways involved in the T-cell-mediated immunity against Epstein-Barr virus: lessons from genetic diseases. Immunological Rev. 2019;291(1):174–89. https://doi.org/10.1111/imr.12791.

Publisher's Note